Bull. Min. Res. Exp. (2019) 158: 217-233

Bulletin of the Mineral Research and Exploration

http://bulletin.mta.gov.tr

Geochemical characteristics of Sabalan volcanic rocks in Northwestern Iran

Reza FAHIM GUILANY[a], Ali DARVISHZADEH[a], Seyed Jamal SHEIKHZAKARIAEE[a*] and Mansour VOSOUGHI ABEDINI[a]

[a] *Department of Geology, Science and Research Branch, Islamic Azad University, Tehran, Iran*

Research Article

Keywords:
Sabalan volcano, calc-alkaline, subduction, geochemistry.

ABSTRACT

Sabalan is a voluminous stratovolcano situated in the northwestern part of Alborz-Azerbaijan zone, 25 km from Meshkinshahr. It is separated by a fault creating a tectonic boundary from Sarab plain and Meshkinshahr. The composition of Sabalan volcanic rocks ranges from andesite, trachyandesite to dacite. The rocks have hypocrystalline porphyritic texture with a glassy matrix and microlite . Plagioclase, amphibole, pyroxene, biotite, and oxides are the main phenocryst phase of the rocks. Some plagioclases show disequilibrium textures (sieve texture and oscillatory zoning). The sieve texture and oscillatory zoning in the plagioclases may be indicative of magma mixing processes in the genesis of the Sabalan volcanic rocks. Geochemical data reveal that the Sabalan lavas exhibit calk-alkaline major-oxide trends with a sodic character and they range in composition from andesite to dacite. Pre-caldera and post-caldera volcanic rocks have similar geochemical features with enrichments in LILE and LREE relative to HFSE and HREE, respectively, and have negative Ti, Nb, and Ta anomalies. Ba/Ta ratios higher than 450 and La/Nb ratios ranging between 2 and 3 indicate a volcanic arc setting for the studied rocks. Based on field and geochemical studies, Sabalan is a subduction-related volcano, occurred as a result of subduction of Neo-Tethyan oceanic crust beneath the Iranian microplate.

Received Date: 26.08.2017
Accepted Date: 24.04.2018

1. Introduction

The Sabalan volcanic field that overlies the northwestern Iran is situated in a continental collision zone between the African-Arabian and Eurasian plates (Ghalamghash et al., 2016) (Figure 1). From early Mesozoic to Quaternary, this collision zone underwent a compressional tectonic regime where compression has stemmed from subduction of Neo-Tethyan oceanic crust underneath the Iranian Central Block, and the subsequent collision between the Arabian and Eurasian plates along the Zagros suture zone (Şengör and Kidd, 1979; Dewey et al., 1986; Dilek et al., 2009; Ghalamghash et al., 2016). Sabalan volcano mountain lies in Qaresou valley in northwest of Ardabil city and extends to the east-west direction, with an approximate length of 60 km and 48 km in latitude to the Fushedagh mountain in the south of Ahar city. It has three peaks along the rough east-west direction. The highest peak is called Soltan Sabalan with a height of 4811 m, and the two other peaks are called Heram or Sabalan-e Kuchak (4740 meters) and Aghan Dagh or Kasra (4600 meters) (Figure 2).

On the northwest and southeast, Sabalan volcano complex is surrounded by NE-SW trending two main faults. Almost half of the linear structures are NW-SE trends, which created the Mou'eel valley on the basis of this trend (Haftani et al., 2008). In addition to the above faults, local faults also divided Sabalan horst into smaller pieces and have contributed to the formation of calderas in this volcano and faulty valleys.

* *Corresponding author: Seyed Jamal SHEIKHZAKARIAEE, j.sheikhzakaria@gmail.com*
https://dx.doi.org/10.19111/bulletinofmre.451565.

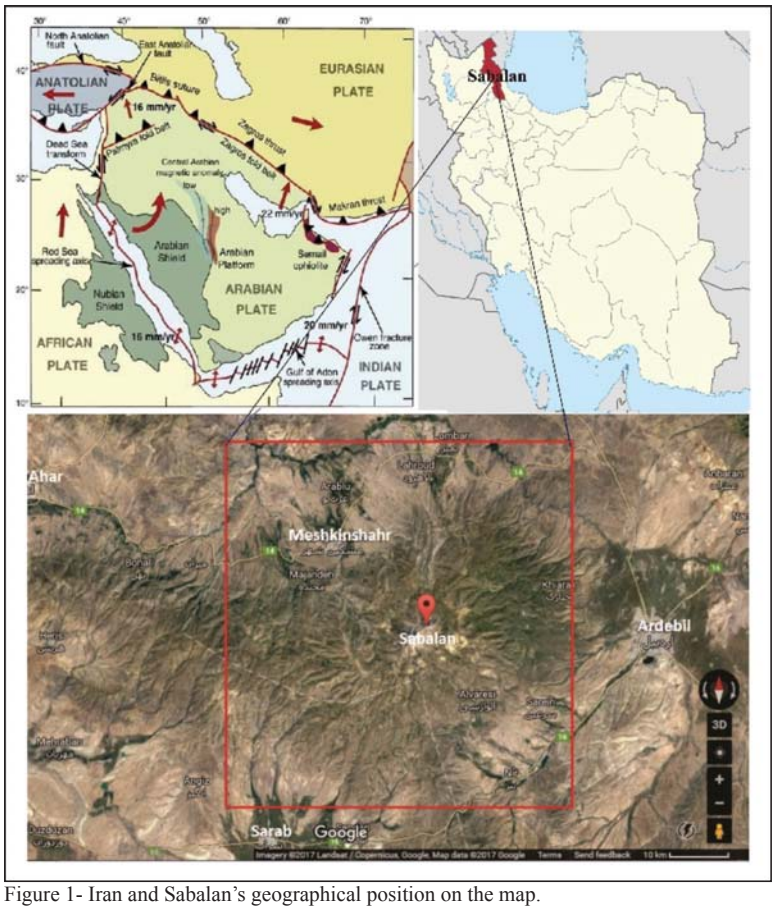

Figure 1- Iran and Sabalan's geographical position on the map.

Figure 2- Three peaks of Sabalan volcano.

This volcano has experienced more than 7 explosive eruptions during its activity (Fahim Guilany, 2016*a*). Sabalan volcanic rocks with calc-alkaline nature are made up of alternation of andesitic and young trachyandesitic to dacitic lavas as the age of Pliocene-Quaternary (Didon and Gemain, 1976; Mousavi, 2013; Shahbazi Shiran and Shafaii Moghadam, 2014; Fahim Guilany, 2016*b*; Ghalamghash et al., 2016). K-Ar absolute dating of Sabalan lavas revealed that Sabalan volcanic activity started at late Miocene (10.4 ± 0.5 Ma) (Alberti et al., 1976; Mousavi, 2013) and continued up to the 110k years ago (Ghalamghash et al., 2016).

One of the most important issues in Sabalan volcanic activity is the presence of pyroclastic air-fall

and base surge deposits, nuée ardentes, and ignimbrites that formed a volume more than 14 km^3 in area (Fahim Guilany et al., 2016) (Figure 3). Because of its potential volcanic hazards and geothermal potential, Sabalan volcano is an imperative object of study.

In this study, petrographical features of the studied rocks are briefly given and the geochemical features of these rocks are discussed in detail. Considering previous studies, the aim of this study is to reveal the nature of chemical variations between andesite and dacite over time (from 10.5 million years ago to 110,000 years ago) as well as discuss the sodic nature of these rocks, which has been previously accepted as potassic.

2. Geology

Sabalan is a voluminous stratovolcano located in the northwestern part of Alborz-Azerbaijan zone and northern part of Bitlis-Zagros suture zone. In the geological map of Meshkinshahr (1:100.000), the volcanic rocks of the area were described as andesite, trachyandesite, and dacite. Sabalan has a collapsed caldera about 12 km in diameter and a depression of about 400 m. The formation of caldera in Sabalan volcano has been considered as the basis for categorization of its important events by the researchers, and its volcanic activities have been divided into two stages: pre-caldera and post-caldera; in terms of the age of its activity, it can be divided into four or even five periods of volcanic activity (Figure 4) as follows:

The first stage (the old series or pre-caldera activity): The volcanic activity of Sabalan was initiated by andesitic eruptions (Figure 5a) during the middle to upper Miocene time (Alberti et al., 1976; Mousavi et al., 2014). According to Mousavi (2013), this age is computed based on andesitic rocks at an altitude of 2200 meters above sea level. During this phase, pyroclastic air-fall deposits with 5 m thickness near Saeen, (around Nir) and the andesitic lavas accumulate into massive thickness with layers of pumice and ash.

The second stage: The most intense volcanic activity of Sabalan dates back to the early Pliocene with trachyandesite lava eruptions (Figure 5b). Radiometric age of these rocks is 5.2 Ma (Mousavi, 2013). During this stage, thick, extensive ash flows

Figure 3- Sabalan pyroclastic deposits; a) Saeen air-fall deposits, b) Sareyn pyroclastic surges, c) Shirvandareh nuée ardentes, d) Chapaqan ignimbrite.

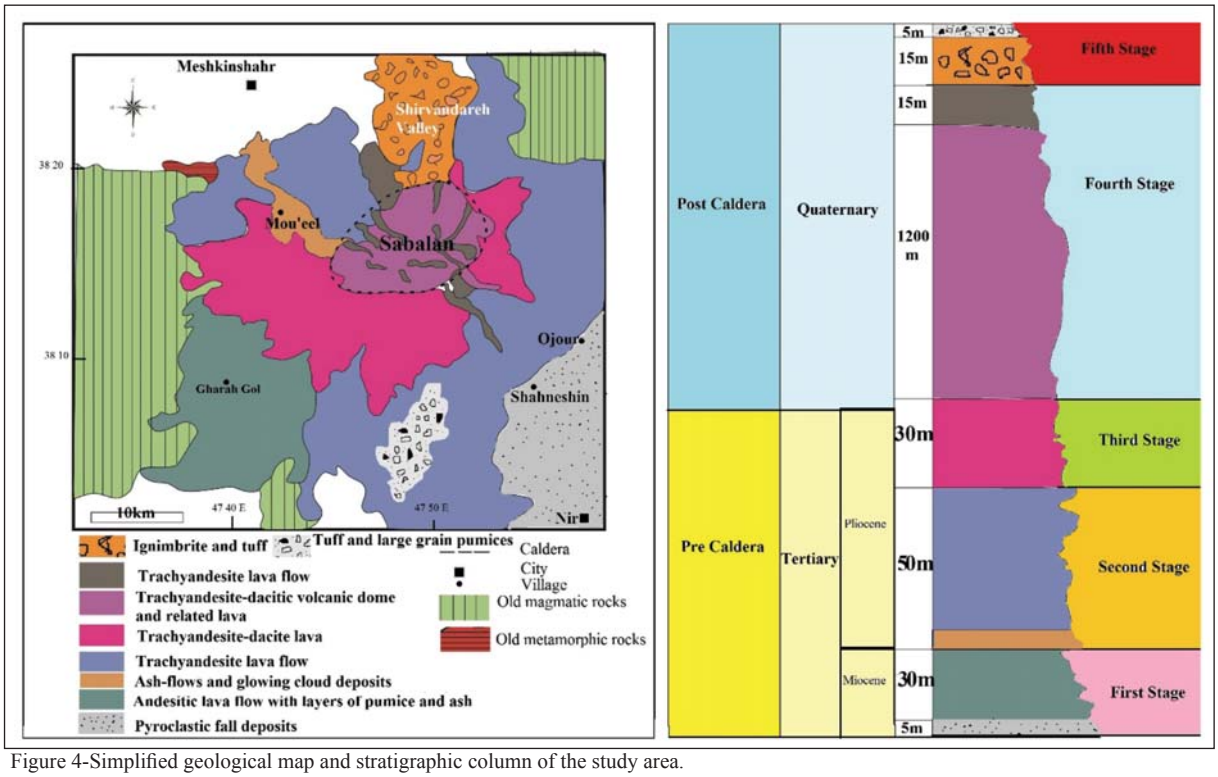

Figure 4-Simplified geological map and stratigraphic column of the study area.

and glowing cloud deposits (Fahim Guilany et al., 2016) as well as lava flows mainly of trachyandesitic composition, erupted possibly from several centers and brought a large volcanic complex reaching a great thickness (Alberti et al., 1976). The above mentioned lavas are more than 50 m thick and spread over 10 km.

The third stage: The evolution of the pre-caldera volcanic sequence with the eruption of a lava flow with the composition of trachyandesite to dacite ends in Sabalan. This lava flow has a fragmental and scrappy morphology with 100 m thickness and a length close to 6 km. The age of these rocks is about 2.8 Ma (Mousavi, 2013).

After pre-caldera eruption, the chamber of magma is discharged and due to the heavy burden of the piled up thick successions of volcanic rocks, the central area collapses and a large caldera develops (Figure 5c). The collapse occurs in two stages in which the second stage, took place with high explosive activity.

The fourth stage or post-caldera activity: This stage, which should be called new series or the post-caldera lavas, actually dates back to the early Quaternary (Alberti, et al., 1976). During this period, immediately after development of the caldera and explosive activities, the volcanic domes, some of which are well preserved and be mostly made up of andesitic to dacitic lava are suspended in the caldera rim (Figure 5d).

The fifth stage: The youngest eruptions of pyroclastic air-fall deposits and ignimbrites occur mainly within the caldera boundaries, and based on Ghalamghash et al. (2016), these tuffs and large grain pumices seen in Sareyn dates back to ca. 110 ka.

3. Methodology

After collecting and providing basic information and records of works done in the study area using aerial photographs and geological maps, all outcrops related to these rocks were identified. These rocks were then systematically sampled in the field during field studies. Eighty-five fresh samples were studied for petrographic investigations. Afterwards, 8 samples were chosen for geochemical analyses at Zarazma lab, Iran. The rock pulps were prepared by using lithium borate fusion for major oxides and ICP-MS (Agilent 4500) for trace and rare earth elements (REE). The results of chemical analyses along with detection limits (DL) are listed in tables 1 and 2. Detection limits were 0.05% for major oxides and 0.02-1 ppm

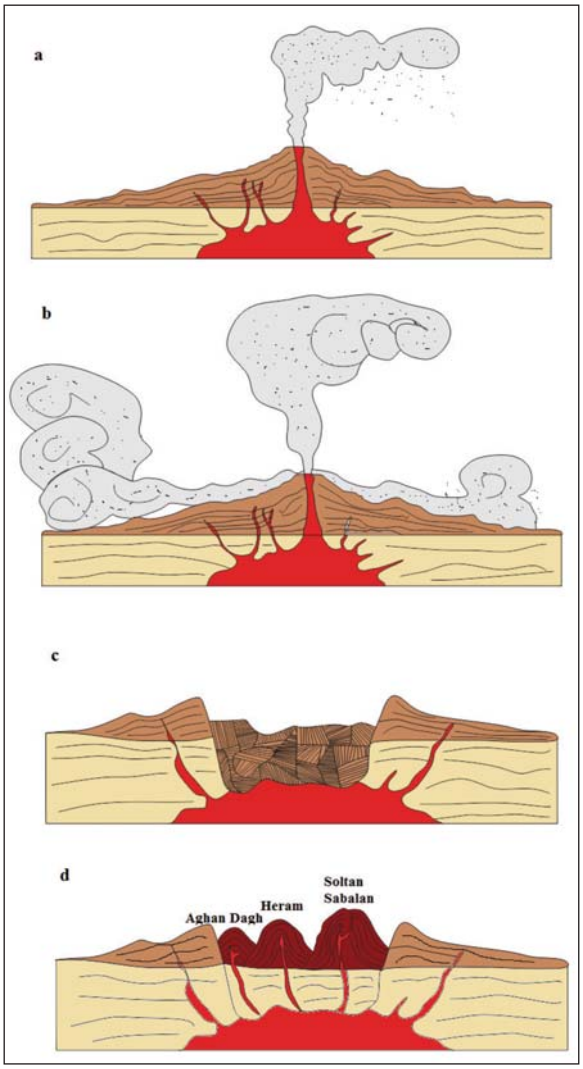

Figure 5- Illustration showing the formation of Sabalan's caldera and pre-caldera and post-caldera volcanic activities; a) pre-caldera explosive eruptions around Nir, b) the most intense pre-caldera volcanic activity of Sabalan, c) caldera subsidence, d) post-caldera series and domes rose in the caldera rim.

for trace elements. The results were compiled using the previously obtained data, and were assessed using software packages such as Igpet 2007 and GCD kit, version 4.1.

4. Results

4.1. Petrography

The lithological differences between the pre-caldera and post-caldera rocks of Sabalan are minor. The pre-caldera series are composed of andesitic to trachyandesitic lavas and the post-caldera series are composed of trachyandesitic to dacitic lavas with minor amount of rhyodacite. The texture of these rocks is porphyritic with glassy to microlitic matrix. Phenocryst phases are plagioclase, amphibole, pyroxene and biotite.

Plagioclase: In some plagioclases, disequilibrium textures such as sieve, dusty, resorbed and oscillatory zoning is observed. Some of the plagioclases have been affected by dissolution and corroded from the margins. The corrosion around plagioclase (Figure 6a) shows physicochemical disequilibrium over magma, and could probably be the result of magma mixing. As mentioned previously, most plagioclases have sieve textures (Figure 6b). There are three theories about the formation of this texture, which are: (a) fast skeletal growth, (b) magma mixing, and (c) rapid drop in pressure or magma decompression. The details related to each of them have been thoroughly discussed by Amini and Jalali (2002). Among these theories, fast skeletal growth does not have many advocates, but in recent studies, two other factors have been introduced and considered the most significant elements in the formation of sieve texture (Mohammadi et al., 2006).

Amphiboles: Amphiboles are observed as euhedral to anhedral crystals, and they are of hornblende type crystals. The most important evidence of disequilibrium in these amphiboles is burned margin texture (Figure 6c). Although Sakoyama (1983) considered this phenomenon to be precipitated by magma mixing, Sigurdsson et al. (2000) related it to resorption of mineral, and magma's rapid rise as well as decrease in steam pressure. Generally, opacitization in amphibole occurs due to a decrease in water pressure (Rutherford and Hill, 1993) or as a result of increase in temperature (Kawabata and Shoutu, 2005; Gill, 2010). The first situation could be associated with magma rise and the second, with magma mixing.

Pyroxene: Augite pyroxene is euhedral to subhedral crystals as both phenocrysts, microphenocrysts and microlites. (Figure 6d).

Biotite: Biotite can be observed as flakes to anhedral in shape with a pleochroism of brown to red and dark brown. On the margin of the biotite, evidences of dissolution border texture can be observed (Figure 6c). Plagioclase and apatite can also be found in these minerals.

Table 1- Results of major-oxide and trace element analysis of the pre-caldera volcanic rocks.

Sample	DL	P1	P2	P3	P4	P5	P6	P7	P8	P9	P10	P11	P12	P13	P14	P15	P16	P17	P18
Wt.%		*				**		***											
SiO_2	0.05	61.34	57.73	57.3	57.2	62.3	61.2	59.2	58.6	60.6	59.8	62.4	52.9	56.7	59.8	62.2	61.5	62.3	62.6
Al_2O_3	0.05	16.59	16.21	16.61	15.6	15.7	14.6	16	16	16.1	15	16.1	17.3	17.3	16.9	17.0	16.8	17.0	16.3
Fe_2O_3[1*]	0.05	4.26	5.58	5.07	5.17	3.78	3.19	4.78	5.54	4.46	3.71	3.26	5.8	5.5	5.05	4.5	3.8	3.8	3.95
CaO	0.05	5.86	6.05	5.15	6.68	4.6	3.42	4.85	4.65	4.3	4.75	4.02	8.2	6.3	5.75	4.65	5.66	5.85	5.2
MgO	0.05	1.97	2.74	2.36	2.58	1.77	1.42	1.98	1.94	1.21	1.78	1.71	3.05	2.5	2.75	2.5	3.3	2.35	2.65
Na_2O	0.05	4.49	5.01	4.7	4.5	4.9	4.3	4.5	4.6	4.6	4.4	4.9	5.1	5.3	4.9	4.1	4.7	5.1	4.75
K_2O	0.05	2.73	2.96	2.46	2.95	2.54	3.14	2.79	3.45	2.96	3.05	2.4	2.3	2.65	2.4	2.15	2.7	2.55	2.4
TiO_2	0.05	0.7	1.35	1.01	0.88	0.61	0.53	0.81	0.9	0.74	0.65	0.63	1.35	1.45	1.05	0.8	1	1.05	0.85
MnO	0.05	0.08	0.05	0.08	0.08	0.06	0.06	0.06	0.08	0.07	0.07	0.06	0.05	0.05	0.1	0.4	0.1	0.1	0.1
P_2O_5	0.05	0.4	0.1	0.72	0.65	0.4	0.34	0.44	0.64	0.38	0.44	0.34	0.1	0.1	0.65	0.1	0.25	0.1	0.5
LOI	0.05	1.4	0.3	1.03	1.99	0.23	4.15	0.87	1.11	0.71	2.4	0.73	1	0.4	0.05	0.8	1.2	0.4	0.35
Ppm																			
Ba	1	715	760	690	730	640	660												
Co	1	11.8	17.1	16.6	16.3	10.8	8.9												
Cs	0.5	2.2	1.4	0.4	2.2	1.4	2.5												
Cu	1	36	56	59	57	36	36												
Dy	0.02	2.39	2.83	2.56	2.73	1.81	1.62												
Er	0.05	1.22	1.35	1.21	1.3	0.83	0.75												
Eu	0.1	1.15	1.87	1.45	1.49	1.1	1.01												
Ga	0.05	19	19	21	19	19	18												
Gd	0.05	3.02	4.48	3.76	4.03	2.73	2.49												
Hf	0.5	2.01	4	4	4	5	3												
Ho	0.05	0.47	0.51	0.48	0.48	0.31	0.29												
Lu	0.1	0.16	0.17	0.2	0.16	0.11	0.12												
Ni	1	22	39	46	41	25	17												
Pr	0.05	6.62	12.4	9.95	10.4	7.6	7.59												
Rb	1	47	57.6	40.8	61.6	53	75.5												
Sn	0.1	0.7	1	1	<1	<1	<1												
Sr	1	927.5	899.2	903	919.5	914.4	911.3												
Tb	0.1	0.46	0.57	0.5	0.51	0.34	0.33												
Th	0.1	13.39	13.6	14.2	14.9	10.8	14.2												
Tm	0.1	0.17	0.19	0.16	0.17	0.12	0.1												
U	0.1	4.12	3.78	3.69	3.43	2.85	4.45												
V	1	75	120	81	92	64	57												
W	1	1.6	2	3	1	1	2												
Y	0.5	11.3	11.3	11.6	12.3	8.3	7.9												
Yb	0.05	1	1.2	1.1	1.1	0.8	0.8												
Zn	1	63	81	82	73	58	56												
Zr	5	87	160	170	160	200	140												
Ag	0.1	0.6	1	1	2	<1	1												
Ce	0.5	73	112	94.3	94.2	73	75.4												
Mo	0.1	3.5	<2	<2	3	<2	3												
Nb	1	15.7	25	25	24	16	19												
Nd	0.5	24.4	44.6	34.6	37.1	26	25.9												
Sm	0.02	4.22	6.6	5.4	5.6	4	3.9												
Tl	0.1	0.2	<0.5	<0.5	<0.5	<0.5	<0.5												
La	1	42	59.9	51.2	51.05	43.02	44.9												
Ta	0.1	1.13	1.6	1.5	1.6	1	1.3												
La/Nb		2.67	2.39	2.04	2.14	2.68	2.36												
Ba/Ta		632	468.7	460	450	640	507.												
La/Yb		42	49.9	46.5	48.8	53.7	56.1												

* Chemical analysis performed by the authors of this study

** Chemical analysis adapted from Mousavi (2013)

** Chemical analysis adapted from Didon and Gemain (1976)

Fe_2O_3-FeO_{total} total

Table 2- Results of major-oxide and trace element analysis of the post-caldera volcanic rocks.

sample	DL	K1	k2	k3	k4	k5	k6	k7	k8	k9	k10	k11	k12	k13	k14	k15
Wt.%		*				**				***					****	
SiO_2	0.05	61.85	60.87	63.02	60.98	61.2	65.4	63.5	65.2	64.6	62.8	64.8	64.4	64.7	62.35	62.89
Al_2O_3	0.05	16.72	16.61	16.87	16.62	16.8	15	14.6	15	15.1	16.2	15.3	16.1	14.3	16.75	16.83
$Fe_2O_3^{2*}$	0.05	3.88	4.96	3.77	3.61	5.09	3.69	3.62	3.75	2.76	3.77	2.99	4.08	2.91	3.38	3.34
CaO	0.05	5.36	6.28	5.04	6.32	5.01	2.62	2.61	2.65	3.12	4.17	3.16	3.99	2.9	4.36	4.2
MgO	0.05	1.96	1.9	1.75	1.81	2.4	1.09	1.08	1.06	1.13	1.81	1.18	1.9	1.18	1.86	1.99
Na_2O	0.05	4.8	4.63	4.9	4.94	3.57	4.11	4.08	4.02	4.6	4.8	4.7	5.3	4.4	5.2	4.98
K_2O	0.05	2.86	2.68	3.	2.81	2.86	4.68	4.17	4.78	3.26	2.7	3.24	3.23	3.5	2.75	2.62
TiO_2	0.05	0.66	0.78	0.63	0.62	0.7	0.7	0.68	0.7	0.46	0.61	0.49	0.68	0.5	0.57	0.55
MnO	0.05	0.07	0.07	0.07	0.07	0.1	0.09	0.09	0.08	0.05	0.06	0.05	0.06	0.05	0.06	0.06
P_2O_5	0.05	0.44	0.31	0.42	0.45	0.27	0.25	0.25	0.25	0.28	0.39	0.3	0.55	0.29	0.4	0.45
LOI	0.05	1.16	0.69	0.27	1.53	1.54	1.32	1.36	1.45	1.7	0.42	1.3	1.08	2.38	1.27	1.2
ppm																
Ba	1	813	638	775	837	844	829	1015	775	630	670	730	810	660		
Co	1	10.5	13.	9.8	11.1					7.1	10.6	7.7	10.6	7.1		
Cs	0.5	1.7	1.6	2.	1.6	2.07	5.07	4.92	4.89	2.6	1.2	2.4	1.9	3.		
Cu	1	31	46	37	36					13.	30	57	17	12.		
Dy	0.02	2.36	2.66	2.23	2.31	3.15	4.06	4.04	4.06	1.39	1.85	1.47	1.8	1.63		
Er	0.05	1.16	1.23	1.03	1.13	1.88	2.48	2.47	2.56	0.78	0.87	0.73	0.86	0.74		
Eu	0.1	1.27	1.24	1.07	1.26	1.29	1.36	1.33	1.35	0.88	1.09	0.95	1.17	0.88		
Ga	0.05									18	19	18	20	17		
Gd	0.05	3.23	3.64	2.96	3.23	4.62	6.27	6.14	6.18	2.28	2.75	2.36	2.85	2.21		
Hf	0.5	2.3	2.76	2.41	2.31	4.9	8.7	8.5	8.7	3.	3.	4.	4.	3.		
Ho	0.05					0.64	0.82	0.84	0.83	0.24	0.33	0.27	0.34	0.29		
Lu	0.1	0.14	0.16	0.13	0.15	0.27	0.41	0.39	0.4	0.09	0.13	0.14	0.09	0.16		
Ni	1	24	23	22	26	28	8.	6.	7.	12.	31	84	24	13.		
Pr	0.05	8.22	7.39	7.16	7.92	7.9	12.45	12.4	12.3	6.57	8.07	7.14	8.47	7.29		
Rb	1	46	53	50	45	72	180.5	173.5	179	77.1	57.1	76.1	65.1	83.9		
Sn	0.1	0.6	0.7	0.7	0.7					<1	<1	<1	<1	<1		
Sr	1	1159.8	899.3	995.4	1164.6	626	401	448	415							
Tb	0.1	0.45	0.51	0.44	0.46	0.61	0.79	0.78	0.78	0.29	0.37	0.33	0.38	0.31		
Th	0.1	10.62	13.82	10.71	10.17	9.28	26.3	25.7	25.8	14.5	11.2	13.4	13.1	17.5		
Tm	0.1	0.16	0.19	0.16	0.15	0.26	0.38	0.36	0.37	0.09	0.12	0.11	0.11	0.11		
U	0.1	3.6	3.3	3.5	3.4	2.75	7.11	6.87	6.98	4.69	3.37	4.22	3.71	5.59		
V	1	68	71	62	71	100	59	58	57	49	85	51	69	42		
W	1	1.2	1.6	1.3	1.3					2.	2.	2.	1.	2.		
Y	0.5	10.3	12.3	9.9	10.6	17.7	23.7	23.5	23.6	7.	8.5	7.4	8.3	7.5		
Yb	0.05	0.9	1.1	0.8	0.8	1.78	2.61	2.58	2.56	0.7	0.8	0.8	0.8	0.8		
Zn	1	62	65	57	63	72	102	72	92	48	62	50	62	50		
Zr	5	98	104	96	102	210	368	356	357	120	140	170	210	130		
Ag	0.1	<0.1	<0.1	<0.1	<0.1					<1	1.	<1	1.	<1		
Ce	0.5	90	81	79	94	78.5	127.5	124.5	125	67.1	77.8	70.3	82.8	73.6		
Mo	0.1	2.8	0.9	2.8	3.1					4.	<2	4.	4.	4.		
Nb	1	17.2	20.4	16.8	17.9	20.9	48.8	47.1	47.5	18	18	17	19	19		
Nd	0.5	29.8	27.2	25.6	28.2	27.6	41.4	41	40.4	21.9	27.2	24.3	28.6	24.2		
Sm	0.02	4.55	4.64	3.98	4.52	4.79	6.61	6.52	6.44	3.1	4.1	3.5	4.3	3.3		
Tl	0.1	0.6	<0.1	0.13	0.39					<0.5	<0.5	<0.5	<0.5	<0.5		
La	1	52	46	47	54	46.6	73.4	71.9	72	40.9	45.4	41.4	48.1	44.5		
Ta	0.1	1.14	1.38	0.94	0.98	1.4	2.4	2.3	1.4	1.3	1.1	1.1	1.1	1.4		
La/Nb		3.02	2.25	2.79	3.01	2.22	1.5	1.5	1.51	2.72	2.52	2.43	2.53	2.34		
Ba/Ta		580.7	462	824.4	854.1	568.1	345.41	441.3	553.5	484.6	609.1	663.6	736.3	471.4		
La/Yb		57.7	41.81	58.7	57.5	26.17	28.12	27.86	28.12	58.4	56.7	51.7	60.1	55.6		

* Chemical analysis performed by the authors of this study

** Chemical analysis adapted from Shahbazi Shiran and Shafaii Moghadam (2014)

*** Chemical analysis adapted from Mousavi (2013)

**** Chemical analysis adapted from Didon and Gemain (1976)

Fe_2O_3-FeO_{total} total

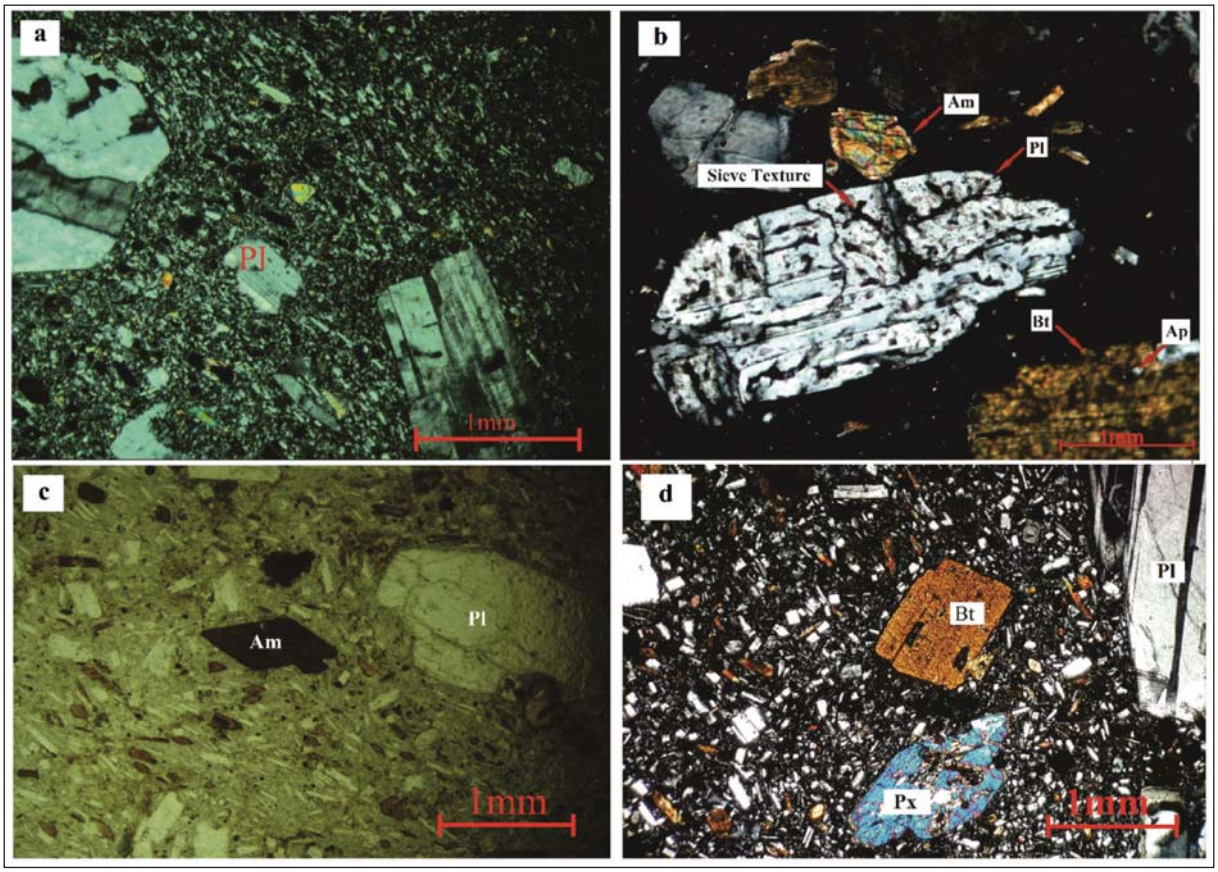

Figure 6- Photomicrographs of; a) Resorbed plagioclase in cross polarised light (XPL), b) Plagioclase with sieve texture in cross polarised light (XPL), c) biotite and opacitized amphibole in plane polarised light (PPL), d) pyroxene and automorph biotite with iron oxides inclusion in cross polarised light (XPL).

4.2. Geochemistry

This study used 33 analyses on pre-caldera and post-caldera rocks series. In addition to the chemical analyses performed by the authors (P1-P4 and K1-K4), chemical analyses conducted by Shahbazi Shiran and Shafaii Moghadam (2014) (K5-K8), Mousavi (2013) (P5-P6 and K9-K13), Didon and Gemain (1976) (P7-P18 and K14-K15) (Tables 1 and 2) were used to make clear assessment by GCDkit software, version 4.1. The samples without trace elements are from Didon and Gemain (1976).

In SiO_2 versus Na_2O+K_2O nomenclature diagram of Le Bas et al. (1986), Sabalan volcanic rocks plot in the field of andesite, trachyandesite, trachydacite and dacite (Figure 7a). In this figure, except for the two samples having alkaline characteristics, the rest are sub-alkaline (Figure 7a). In order to determine the tholeiitic and/or calc-alkaline characteristics of this sub-alkaline series, the AFM diagram (Irvine and Baragar, 1971) has been plotted. It is clear from the figure that the sub-alkaline samples plot on the fractionated calc-alkaline field (Figure 7b).

Calc-alkaline rocks included basalts and andesites that have more alumina (wt% 20-16 = Al_2O_3) and are found in the orogenic belts and rocks related to the island arc. This group of rocks has a clear association with subduction zones and are originally generated in compressional tectonic type (Philpotts, 1990).

The major element variations against SiO_2 for Sabalan volcanic rocks are presented in the form of Harker's (1909) diagram (Figure 8). Similar geochemical behaviours observed in figure 8 indicate that the pre-caldera and post-caldera rocks have a same parental magma and have been fed from one magma chamber. Furthermore, based on the trends of increasing K_2O and SiO_2 and decreasing TiO_2, MgO, FeO, CaO in Harker's diagrams, post-caldera rocks are more differentiated than pre-caldera types. Since MgO contents of all the samples is very low, the volcanic rocks region cannot be suggested to have induced the

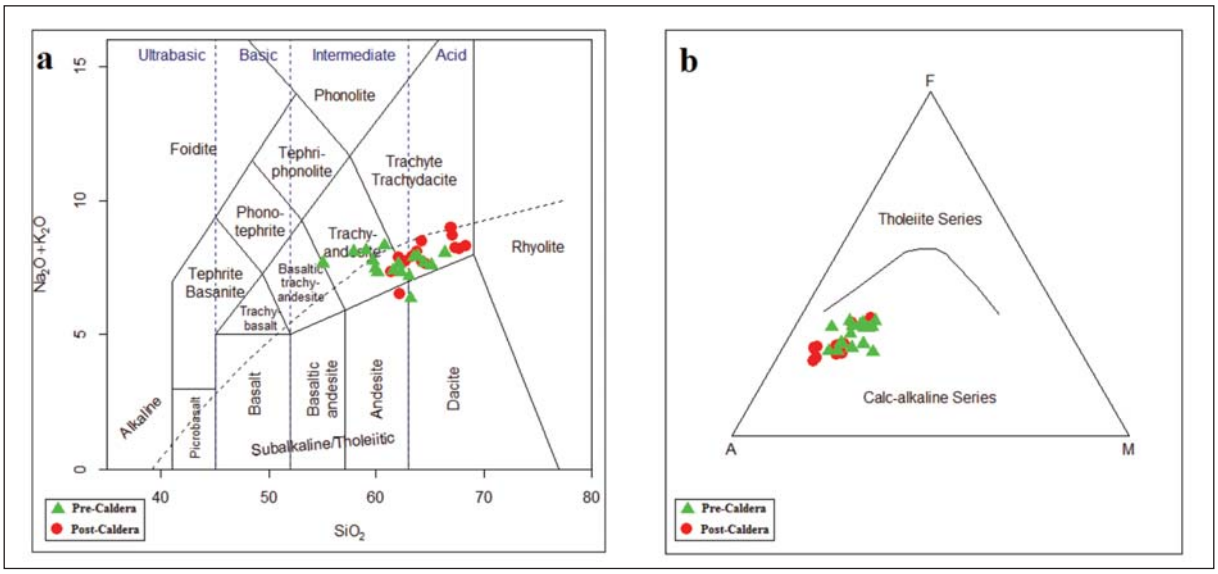

Figure 7- a) Total alkali versus SiO_2 plot for Sabalan volcanic rocks, all values as weight % (Le Bas et al., 1986), b) AFM diagram (Irvine and Baragar, 1971) for Sabalan sub-alkaline samples.

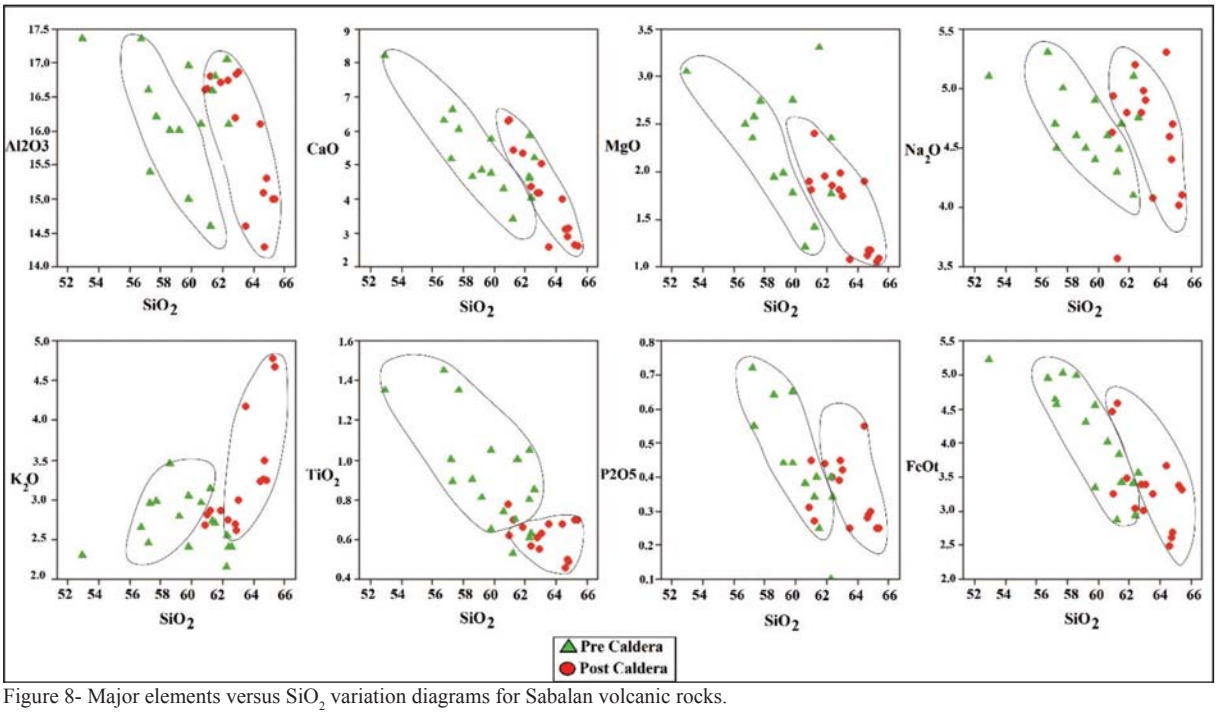

Figure 8- Major elements versus SiO_2 variation diagrams for Sabalan volcanic rocks.

partial melting of peridotite mantle parental magma (Rollinson, 1993). Descending trend of P_2O_5, CaO, FeO, MgO and TiO_2 oxides in post-caldera rocks in comparison with pre-caldera rocks can to some extent be associated with differentiation and crystallization of plagioclase, ferromagnesian minerals (such as olivine and pyroxene), and oxide minerals (such as ilmenite and titano-magnetite) as well as apatite in the location of magma settlement of these rocks. The Al_2O_3 variations in pre-caldera rocks is regular and relatively fixed, but in post-caldera rocks with higher proportion of silica, a slight decrease in trend is visible. The variations in Al_2O_3 can be reflect the removal of Ca-plagioclase during fractional crystallization.

4.3. The Origin

Determination of the tectonic setting of rocks is highly essential in the interpretation of their petrogenesis. To determine and identify the tectonic setting of igneous rocks, the tectonic discrimination diagrams have been used. The diagrams are mostly based on rare earth elements, and immobile elements or elements with low mobility are usually used. Since the high field strength elements (HFSE) such as Zr, Nb, Y, P, and Ti are relatively immobile in aqueous fluids and are stable during weathering, these elements are highly applicable.

Chondrite-normalized (Thompson, 1982) trace element spider diagram of Sabalan volcanic rocks is presented in figure 9a. As can be observed in this figure, the interesting patterns indicate negative anomalies in Nb and Ti and positive peaks in K, Rb, Th, and U, which are characteristic of arc magmas in subduction zones. Enrichment in U and Th in the spider diagrams may be due to the addition of pelagic sediments and/or altered oceanic crust to the source of magma (Fan et al., 2003).

Chondrite-normalized (Nakamura, 1974) rare earth element patterns of the Sabalan volcanic rocks can be seen in figure 9b. Sabalan volcanic rocks are enriched in light rare elements (LREE) (from La to Sm) relative to heavy rare earth elements (HREE), and they also show flat patterns from Dy to Lu. Enrichment in LREE relative to HREE and the low TiO_2, Zr and Nb contents demonstrate the dependency of these rocks on calc-alkaline series (Machado et al., 2005). Eu element showed slight negative anomalies, which was probably related to the existence of plagioclases as the main phenocryst found in the rocks of the region.

Based on tectonic discrimination diagrams (Muller and Groves, 1997), volcanic rocks of the study area are placed within the range of the subduction related magmatic arcs (Figure 10a and b). Additionally, in the Th/Hf versus Ta/Hf diagram (Schandl and Gorton, 2000) (Figure 10c), the studied samples are in the range of active continental margin, and in the (Zr*3)-(Nb*50)-(Ce/P_2O_5) triangular diagram (Muller and Groves, 1997), all samples plot in the field of post-collisional arc zone (Figure 10d). Considering the geochemical characteristics, and taking into account the spatial and temporal position of Sabalan volcano, it seems that these rocks were formed from subduction of Neo-Tethyan oceanic crust under the Iranian microplate and are formed in an arc magmatic zone.

5. Discussion

Three main geodynamic models have been proposed to clarify the melting process of the lithospheric mantle in NW Iran and SE Turkey. They include mantle plume (Ershov and Nikishin, 2004), lower crust delamination (Pearce et al., 1990) and slab break off (Keskin, 2003; Şengör et al., 2003, Ghalamghash et al., 2016). There is no evidence of a mantle plume originating in NW Iran; thus, the melting of mantle lithosphere by heat from a mantle plume is improbable (Dabiri et al., 2011). Although the study of Pearce et al. (1990) in young volcanoes in SE Turkey and the study of Liotard et al. (2008) in the genesis of Quaternary alkaline volcanic rocks in Damavand volcano, proposed lower crust delamination for upper

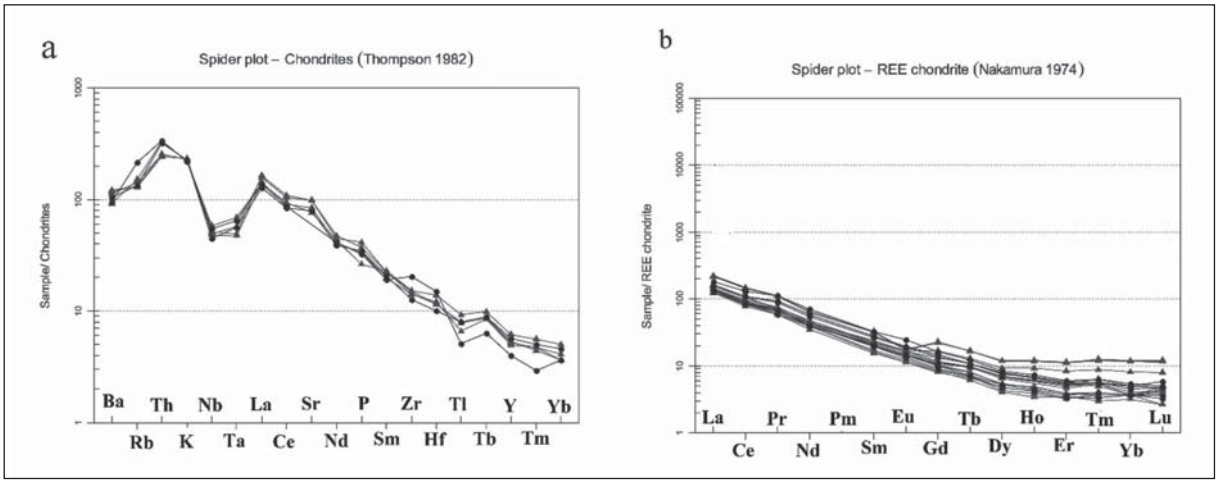

Figure 9- a) Chondrite-normalized (Thompson, 1982) spider diagram, b) Chondrite-normalized (Nakamura, 1974) REE diagram for studied samples.

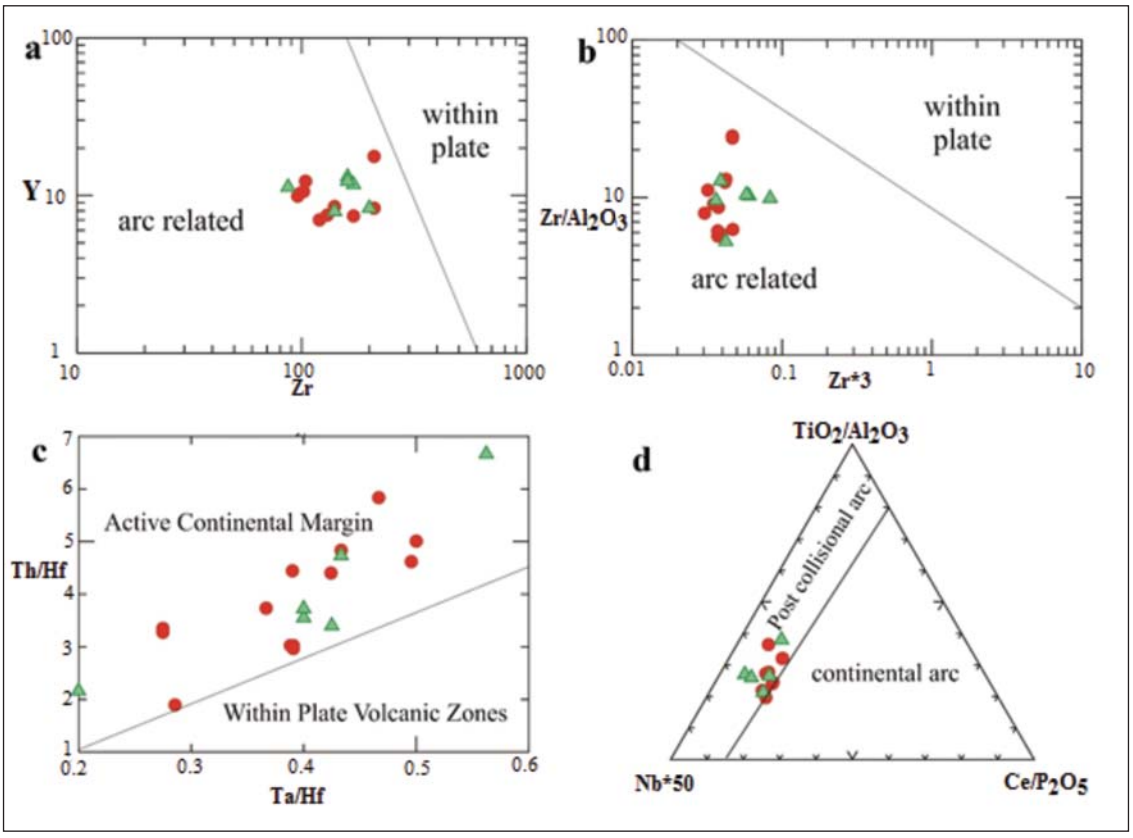

Figure 10- a) Zr-Y diagram (Muller and Groves, 1977); b) Zr/Al_2O_3 – Zr*3 diagram (Muller ve Groves, 1997); c) Th/Hf against Ta/Hf diagram (Schandl and Gorton, 2000) and d) (Zr*3)-(Nb*50)-(Ce/P_2O_5) triangular diagram (Muller and Groves, 1997) of Sabalan volcanic rocks.

Cenozoic magmatism in eastern Turkey and NW Iran. Keskin et al. (2006) and Şengör et al. (2003) suggested that Neo-Tethyan oceanic slab break off under the Eurasia plate was the trigger the Quaternary magmatism in this area (Ghalamghash et al., 2016). Also Neil et al. (2013) proposed that slab break off and perhaps some lithospheric delamination is applicable to Armenia, Eastern Anatolia and NW Iran. Since the slab remnant has been tomographically detected in seismic studies (Gök et al., 2003; Zor et al., 2003; Lee and Zaho, 2007), we tentatively support the model of oceanic crust break off.

Both pre-caldera and post-caldera volcanic rocks share the same geochemical features, indicating that they are probably derived from a long-lived and homogeneous source which produce similar parental magmas. All Sabalan rocks have low MgO (<1.35 wt.%), and direct derivation via partial melting of peridotite mantle parental magma is impossible. High amount of Al_2O_3 in chemical analysis seems logical considering the high amount of plagioclase in the samples. In addition, in intermediate calc-alkaline series, the amount of Al_2O_3 is almost 13 to 16 wt %, which is consistent with the samples' analyses. Except for three samples, in all the samples the amount of Na_2O is more than K_2O (Na_2O/K_2O>1) (Figure 11). This is due to the higher amount of sodic plagioclases in contrast to potassium minerals such as biotite, hornblende and sanidine.

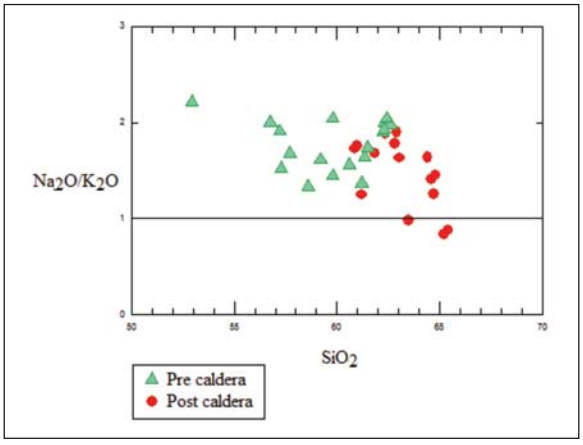

Figure 11- Na_2O/K_2O – SiO_2 diagram of the pre-caldera and post-caldera rock series.

Based on systematic variations in the major elements with increasing SiO_2, fractional crystallization (FC) is identified as a major factor controlling the compositional diversity, but the interaction with crustal rocks along with derivation from a subduction contaminated source for the Sabalan volcanic rocks is also clear from Th/Yb vs. Ta/Yb diagrams (after Pearce, 1983) (Figure 12a). As shown in figure 12a, the volcanic rocks of Sabalan plot in the field of active continental margins and a higher Th content could also result from interaction of ascending lavas with crustal rocks through the process of assimilation fractional crystallization (AFC). In addition, over the compositional range from andesite to dacite, AFC modeling (Figure 12b) suggests that crustal assimilation is negligible due to the very low r values ($r < 0.1$; r = rate of assimilation to rate of fractional crystallization). The results of AFC modeling for volcanic rocks of Sabalan also showed that the degree of magma crust interaction is larger in post-caldera samples (more evolved lavas) than the pre-caldera samples.

Phenocryst assemblages in Sabalan volcanic rocks (plagioclase + amphibole + pyroxene + biotite for pre-caldera series and plagioclase + amphibole ± alkali-feldspar ± quartz for post-caldera series) suggest that amphibole and plagioclase could have been important fractionating phases. Also Geochemical data are also consistent with these petrographic observations: Pre-caldera rocks show a positive correlation in the Rb vs. Y diagram which is consistent with fractionation of plagioclase + clinopyroxene (Pl + Cpx) or plagioclase + amphibole (Pl + Amp) whereas the horizontal or slightly negative trend shown by the post-caldera rocks suggests that the lavas containing hydrous minerals (e.g., amphiboles) display distinct depletion with increasing Rb (Figure 13).

In figure 14, MORB (mid-ocean ridge basalts)-normalized trace element spider diagram of the Sabalan volcanic rocks in northwest Iran is compared with the spider diagram of the Erzurum-Kars plateau volcanic rocks in the east of Turkey (Keskin et al., 1998). The Erzurum-Kars plateau volcanoes in eastern Turkey were described as volcanoes of the type formed after collision (Keskin et al., 1998). The enrichment with LREE and LILE relative to HSFE, and the negative anomalies in Nb and Ta and low values of Y, Ti and Yb are the geochemical characteristics of these two regions.

Ba/Ta ratio greater than 450 and La/Nb ratios of 2-7 are also indicative of the magmas generated in a volcanic arc setting (Gill, 1981; Macdonald et al., 2001). Ba/Ta and La/Nb ratios in Sabalan volcanic rocks are 450-854.1 and 2.04-3.02, respectively. Zr/Y ratio can also be used in determining the tectonic setting (Pearce and Norry, 1979). Accordingly, Zr/Y ratio of continental volcanic arc rocks is generally greater than 3, whereas this ratio is less than 3 in oceanic volcanic arcs. The volcanic rocks of the study area have a Zr/Y ratio more than 3, typical of continental volcanic arc rocks. This ratio for Sahand (another volcano of this region) volcanic rocks is about 19 (Pirmohammadi Alishah et al., 2012). The high La/Yb ratio (from 26 to 60) and the relatively high $(La)_N$ (from 42 to 73) and

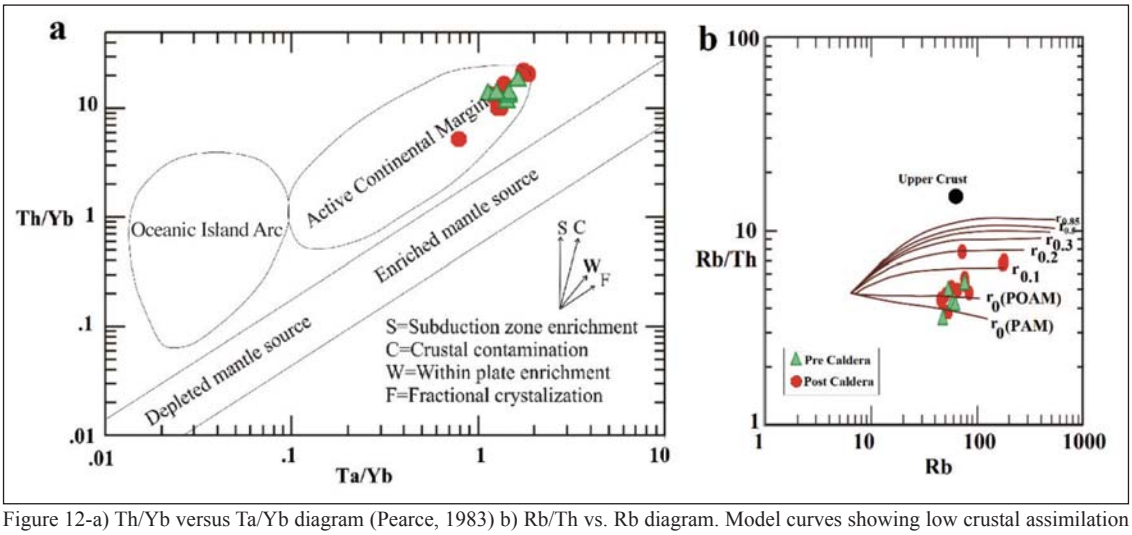

Figure 12-a) Th/Yb versus Ta/Yb diagram (Pearce, 1983) b) Rb/Th vs. Rb diagram. Model curves showing low crustal assimilation in Sabalan volcanic rocks.

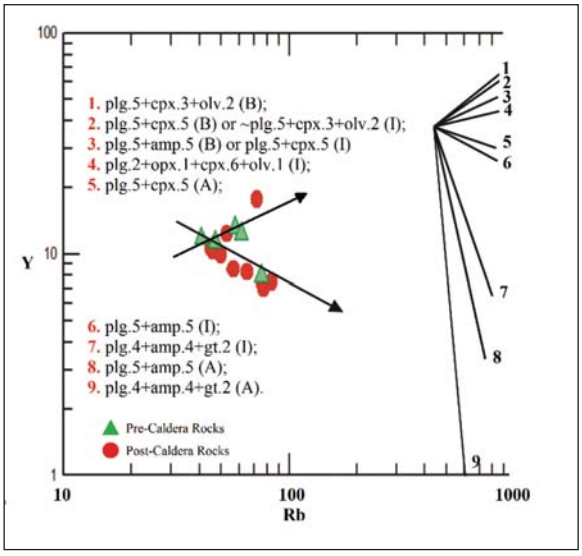

Figure 13- Rb vs. Y model diagram for hydrous (amphibole) vs. anhydrous (clinopyroxene) fractional crystallization. plg: plagioclase, cpx: clinopyroxene, opx: orthopyroxene, olv: olivine, amp: amphibole, gt: garnet. B: basic, I: intermediate, and A: acid magma compositions.

and low magnesium number of the region's rocks substantiate the relevance of these lavas to active continental margins. Since andesites and dacites often belong to mature arcs of continental margin, the existence of ignimbrite deposits with a composition of ryholitic-ryhodacitic in Sabalan's volcano (Fahim Guilany, 2016*a*) shows its relevance to a mature magmatic arc. Accordingly, the tectono-magmatic setting of the study area can be considered as an active continental margin. The Turkish-Iranian high plateau is bounded on the north by the eastern Pontide arc and the lesser Caucasus magmatic belt and is bordered on the south by continental blocks including Bitlis-Pütürge- Sanandaj-Sirjan blocks (Shahbazi Shiran and Shafaii Moghadam, 2014). Such Pliocene-Quaternary volcanic cones and flows as Nemrut, Ararat, Sabalan and Sahand are prevalent in this plateau, and most of them indicate post-collisional affinities (Riou et al., 1981; Özdemir et al., 2006) which substantiates the above results.

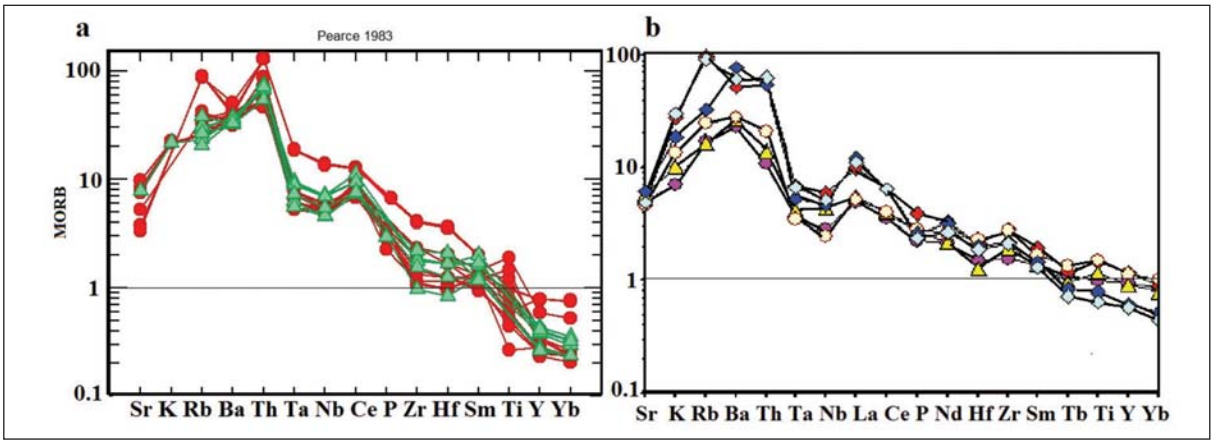

Figure 14- Comparison of MORB (mid-ocean ridge basalts)-normalized trace element spider diagram of the Sabalan volcanic rocks; a) with the Erzurum-Kars Plateau in the east of Turkey, b) (Keskin et al., 1998).

low $(Yb)_N$ (from 0.7 to 2.6) in Sabalan volcanic rocks indicate that they were originated from low degrees of partial melting of enriched mantle. This enrichment is due to the addition of aqueous fluids derived from dehydration of the subducted oceanic crust to lithospheric mantle under Sabalan. The Sm/Yb vs. La/Sm diagram (Figure, 15) (Bezard et al., 2011) has been used to determine the partial melting degrees of the mantle source from which the Sabalan lavas were originated. It is assumed that these rocks are generated from low degree of partial melting (<0.1) similar to Quaternary lavas reported in western Iran (Allen et al., 2013) from lithospheric mantle source, with a composition that supposedly correspond to clinopyroxene-garnet lherzolite. Also Neil et al. (2013) in their study of Turkish-Armenian-Iranian plateau, proposed that magmas in this region are derived from low-degree melting of a shallow, subduction-modified lithospheric mantle source.

The Ba/Nb ratios of the samples range between 31.27 and 47.26. Ba/Nb ratio of the active continental margin magmatism is generally greater than 28 (Gill, 1981; Fitton et al., 1988). Thus, these high Ba/Nb ratios are characteristics of magmatism in active continental margins. Evidence such as the explosive nature of volcanoes in the region, volcanic breccia deposits, agglomerate, acidic tuffs, ignimbrites

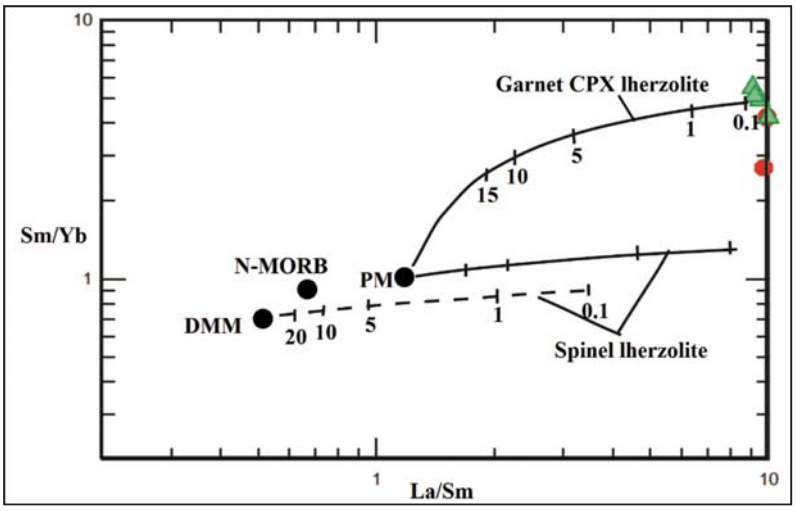

Figure 15-The Sm/Yb vs. La/Sm diagram (Bezard et al., 2011) for Sabalan volcanic rocks. The melting curves were obtained using the non-modal batch melting equations of Shaw (1970), DMM (Depleted MORB Mantle) is from Salters and Stracke (2004), PM (Primitive mantle) is from Sun and McDonough (1989). Spinle lherzolite (with mode and melt mode of olivine (53.3%) + orthopyroxene (27%) + clinopyrocene (17%) + spinel (3%) (Kinzler, (1997)), and garnet-clinopyroxene peridotite (with mode and melting mode of olivine (53.3%) + Clinopyroxene (35.7%) +garnet (11%) (Walter, 1998)) are the source of the melting. Partition coefficients are from McKenzie and O'Nions (1991) (see table 3). Tick marks show the degree of partial melting (%) of the different sources.

Table 3- Partition coefficient values used in the melting models.

	Olivine	Orthopyroxene	Clinopyroxene	Spinel	Garnet
Sm	0.0013	0.01	0.26	0.01	0.217
Yb	0.0015	0.049	0.28	0.01	4.03
La	0.0004	0.002	0.054	0.01	0.01

6. Conclusion

With regard to the long-term activity of Sabalan, it must be accepted that its magma was differentiated in magma chamber. As a result, the initial alkaline andesite under the influence of fractional crystallization turned into intermediate compositions of trachyandesite, trachydacite and dacite. Based on higher SiO_2 in post-caldera rocks compared to pre-caldera rocks, the post-caldera phase generally produced more magma constituents. On the basis of the geochemical data of major and rare elements, Sabalan volcanic rocks are considered to be calc-alkaline. The Zr/Y ratio shows that the studied rocks are related to continental volcanic arcs. In spider plots, Rb, Ba, and K showed enrichment and Nb and Ti showed depletion, which are indicative of magmatic arcs in subduction zones. Therefore, taking into account the spatial and temporal position of volcanic rocks of the area, it seems that these rocks were formed from subduction of Neo-Tethyan oceanic crust under the Iranian microplate and are formed in an arc magmatic zone in the Quaternary.

References

Alberti, A.A., Comin-Chiaramonti, P., Dibattistini, G., Nicoletti, M., Petrucciani, C., Siniqoi, S. 1976. Geochronology of the eastern Azarbaijan volcanic plateau (north-west Iran). Rendiconti della Societa Italiana di Mineralogia e Petrologia 32, 579-589.

Allen, M.B., Kheirkhah, M., Neill, I., Emami, M.H., McLeod, C.L. 2013. Generation of arc and within-plate chemical signatures in collision zone magmatism: Quaternary lavas from Iran. Journal of Petrology 54, 887-911.

Amini, S., Jalali, M. 2002. Sieve texture in plagioclase and its importance in the interpretation of petrological evidence of volcanic rocks in the North East Qorveh. Journal of Sciences Islamic Azad University (JSIAU) 12, 44, 3521-3535.

Bezard R., Hebert R., Wang C., Dostal J., Dai J., Zhong H. 2011. Petrology and geochemistry of the Xiugugabu ophiolitic massif, western Yarlung Zangbo suture zone, Tibet. Lithos 125, 347-367.

Dabiri, R., Emami, M.H., Mollaei, H., Chen, B., Abedini, M.V., Omran, N.R., Ghaffari, M. 2011. Quaternary post-collision alkaline volcanism NW of Ahar (NW Iran): Geochemical Constraints of Fractional Crystallization Process. Geologica Carpathica 62, 547-562. Doi: org/10.2478/v10096-011-0039-2

Dewey, J.F., Hempton, M.R., Kidd, W.S.F., Şaroğlu, F., Şengör, A.M.C. 1986. Shortening of continental lithosphere: The neotectonics of Eastern Anatolia — a young collision zone. Coward, M., Ries, A. (Ed.). Collision Tectonics. Special Publication of the Geological Society. London, 19, 3-36.

Didon, J., Gemain, Y.M. 1976. Le Sabalan, Volcan Plio-quaternair de l'Azerbaidjan oriental (Iran); etude geologique et petrographique de l'edifice et de son environnement regional, These de 3eme Cycle, University, 304 p. Grenoble (unpublished).

Dilek, Y., Imamverdiyev, N.A., Altunkaynak, S. 2009. Geochemistry and tectonics of Cenozoic volcanism in the Lesser Caucasus (Azerbaijan) and the peri-Arabian region: Collision induced mantle dynamics and its magmatic fingerprint. International Geology Review 143, 536-578. Doi: 10.1080/00206810903360422.

Ershov, A.V., Nikishin, A.M. 2004. Recent geodynamics of the Caucasus Arabia, East Africa Region. Geotectonics 38, 2, 123-136.

Fahim Guilany, R. 2016*a*. Sabalan: The most complex volcano in Iran. Third International Conference of Geographical Sciences, Al-Khwarizmi Higher Institute of Science and Technology, Shiraz, Iran.

Fahim Guilany, R. 2016*b*. The pyroclastic deposits of Sabalan volcano. Ph.D. Dissertation, Geology Department, Research and Science Branch, Islamic Azad University, 223 p. Tehran (unpublished).

Fahim Guilany, R., Darvishzadeh, A., Sheikhzakariaee, S.J. 2016. The Nuee Ardentes of Sabalan volcano in Iran. Open Journal of Geology 6, 1553-1566. Doi: org/10.4236/ojg.2016.612110_

Fan, W.M., Guo, F., Wang, Y.J., Lin, G. 2003. Late Mesozoic calc-alkaline volcanism of post-orogenic extension in the northern Da Hinggan Mountains, northeastern China. Journal of Volcanology and Geothermal Research 121, 115-135.

Fitton, J. G., James, D., Kempton, P.D., Ormerod, D.S., Leeman, W.P. 1988. The role of lithospheric mantle in the generation of late Cenozoic basic magmas in the Western United States. J. Petrol., Special Lithosphere Issue, 331-349.

Ghalamghash, J., Mousavi, S.Z., Hassanzadeh, J., Schmitt, A.K. 2016. Geology, zircon geochronology, and petrogenesis of Sabalan volcano (northwestern Iran). Journal of Volcanology and Geothermal Research 327, 192-207. Doi: 10.1016/j.jvolgeores.2016.05.001.

Gill, J.B. 1981. Orogenic andesites and plate tectonics. Springer - Verlag, New York.

Gill, R. 2010. Igneous Rocks and Processes: A Practical Guide. Wiley-Blackwell, Chichester, 428 p.

Gök, R., Sandvol, E., Turkelli, N., Seber, D., Barazangi, M. 2003. Sn attenuation in the Anatolian and Iranian plateau and surrounding regions. Geophysical Research Letters 30, 24, 8043. Doi: 10.1029/2003GL018020

Haftani, M., Bohloli, B., Ellassi, M., Talebi, B. 2008. In-situ stress determination in Sabalan geothermal reservoir. 2nd IASME/ WSEAS International Conference on Geology and Seismology, World Scientific and Engineering Academy and Society, Cambridge, U.K., 88-93.

Harker, A. 1909. The Natural History of Igneous Rocks. Methneu, London, 344 p.

Irvine, T.N., Baragar, W.R.A. 1971. A guide to the chemical classification of the common volcanic rocks. Canadian Journal of Earth Sciences 8, 523-548.

Kawabata, H., Shuto, K. 2005. Magma mixing recorded in intermediate rocks associated with high-Mg andesites from the Setouchi volcanic belt, Japan: Implications for Achenn TTG Formation. Journal of Volcanology and Geothermal Researches 140, 241-271.

Keskin, M. 2003. Magma generation by slab steepening and breakoff beneath a subduction-accretion complex: An alternative model for collision-related volcanism in eastern Anatolia. Geophysical Research Letters 30, 24, 1-9. Doi: 10.1029/2003GL018019.

Keskin, M., Pearce, J.A., Mitehell, J.G. 1998. Volcano stratigraphy and geochemistry of collision-related volcanism on the Erzurum-Kars plateau, northeastern Tuerkey. Journal of Volcanology and Geothermal Research 85, 355-404.

Keskin, M., Pearce, J.A., Kempton, P.D., Greenwood, P. 2006. Magma-crust interactions and magma plumbing in a post-collisional setting: Geochemical evidence from the Erzurum-Kars volcanic plateau, eastern Turkey. Dilek, Y., Pavlides, S. (Ed.). Post-collisional Tectonics and Magmatism in the Mediterranean Region and Asia. Special Papers -- Geological Society of America, 409, 475-505.

Kinzler, R.J., 1997. Melting of mantle peridotite at pressures approaching the spinel to garnet transition: application to midocean ridge basalt petrogenesis. Journal of Geophysical Research 102, 853–874.

Le Bas, M.J., Le Maitre, R.W., Streckeisen, A., Zannetin, B.A. 1986. Chemical classification of volcanic rocks based on the total alkali-silica diagram. Journal of Petrology 27, 745-750.

Lee, J.S., Zhao, D.P. 2007. Teleseismic evidence for a break-off subducting slab under Eastern Turkey. Earth and Planetary Science Letters 257, 14-28.

Liotard, J.M., Dautria, J.M., Bosch, D., Condomines, M., Mehdizadeh, H., Ritz, J.F. 2008. Origin of the absarokite-banakite association of the Damavand volcano (Iran): Trace elements and Sr, Nd, Pb isotope constraints. International Journal of Earth Sciences 97, 89-102.

Macdonald, R., Hawkesworth, C.J., Heath, E. 2001. The lesser Antilles volcanic chain: A study in arc magmatism. Earth Science Reviews 49, 1-76.

Machado, A., Lima, E.F., Chemale, J.F., Morta, D., Oteiza, O., Almeida, D.P.M., Figueiredo, A.M.G., Alexandre, F.M., Urrutia J.L. 2005. Geochemistry constraints of Mesozoic-Cenozoic calc-alkaline magmatism in the South Shetland arc, Antarctica. Journal of South America Earth Sciences 18, 407-425.

McKenzie, D., O'Nions, R.K. 1991. Partial melt distributions from inversion of rare earth element concentrations. Journal of Petrology 32, 1021–1091.

Mohammadi, R., Emami, M.H., Vosoughi Abedini, M. 2006. Petrography and petrology of oligo-miocene lavas of Hamedan Razn Region. Journal of Fundamental Sciences of Islamic Azad University 61, 1-18.

Mousavi, G. 2013. The volcanology and petrology of Sabalan volcano, North West of Iran. Ph.D. Dissertation, Geology Department, Research and Science Branch, Islamic Azad University, 195 p. Tehran (unpublished).

Mousavi, S.Z., Darvishzadeh, A., Ghalamghash, J., Vosoughi Abedini, M. 2014. Volcanology and geochronology of Sabalan volcano, the highest stratovolcano in Azerbaijan region, NW Iran. Nautilus 128, 3-1, 85-98.

Muller, D., Groves, D.L. 1997. Potassic igneous rock and associated gold-copper mineralization. Bhattacharji, S., Friedman, G.M., Neugebauerand, H.J., Seilacher, A. (Ed.). Lecture Notes in Earth Sciences 56, 238 p.

Nakamura, N. 1974. Determination of REE, Ba, Fe, Mg, Na and K in carbonaceous and ordinary chondrites. Geochimica et Cosmochimica Acta 38, 757-775.

Nakamura, N. 1977. Determination of REE, Ba, Mg, Na and K in carbonaceous and ordinary chondrites. Geochemica et Cosmochimica Acta 38, 757-775.

Özdemir, Y., Karaoğlu, Ö., Tolluoğlu, A.U., Güleç, N. 2006. Volcanostratigraphy and petrogenesis of the Nemrut stratovolcano, East Anatolian High Plateau: the most recent post-collisional volcanism in Turkey. Chemical. Geology. 226, 189-211.

Pearce, J.A. 1983. Role of sub-continental lithosphere in magma genesis at active continental margins. In: Hawkesworth, C.J. and Norry, M.J. (eds) Continental basalts and mantle xenoliths, Shiva, Nantwich, pp 230-249.

Pearce, J.A., Norry, M.J. 1979. Petrogenetic implications of Ti, Zr, Y and Nb variations in volcanic rocks. Contributions to Mineralogy and Petrology 69, 33-47.

Pearce, J.A., Bender, J.F., De Long, S.E., Kidd, W.S.F., Low, P.J., Güner, Y., Şaroğlu, F., Yılmaz, Y., Moorbath, S., Mitchell, J.G. 1990. Genesis of collision volcanism in Eastern Anatolia, Turkey. Journal of Volcanology Geothermal Research 44, 189-229.

Philpotts, A.R. 1990. Principles of Igneous and Metamorphic Petrology. Prentice Hall, New Jersey, 498 p.

Pirmohammadi Alishah, F., Ameri, A., Jahangiri, A., Mojtahedi, A., Keskin, M. 2012. Petrology andgeochemistry of volcanic rocks from the south of Tabriz (Sahand volcano). Petrology 9, 1, 37-56.

Riou, R., Dupuy, C., Dostal, J. 1981. Geochemistry of coexisting alkaline and calc-alkaline volcanic rocks from northern Azarbaijan (N.W. Iran). Journal of Volcanology and Geothermal Research 11, 253-275.

Rollinson, H. 1993. Using Geochemical Data: Evolution, Presentation, Interpretation. Longman Scientific and Technical, London, 352 p.

Rutherford, M., Hill, P. 1993. Magma ascent rates from amphibole breakdown: An experimental study applied to the 1980-1986 Mount St. Helens eruptions. Journal of Geophysical Research 98, B11, 19667-19685.

Sakoyama, M. 1983. Petrology of arc volcanic-rocks and their origin by mantle diapirs. Journal of Volcanology and Geothermal Research 18, 297-320.

Salters, V.J.M., Stracke, A. 2004. Composition of the depleted mantle. Geochemistry, Geophysics, Geosystems 5, Q05B07.

Schandl, E.S., Gorton, M.P. 2000. Form continents to island arcs: A geochemical index of tectonic setting for arc-related and within-plate felsic to intermediate volcanic rocks. The Canadian Mineralogist 38, 1065-1073.

Şengör, A.M.C., Kidd, W.S.F. 1979. Post-collision tectonics of the Turkish and Iranian plateau and companions with Tibet. Tectonophysics 55, 3, 261-376.

Şengör, A.M.C., Özeren, S., Zor, E., Genç, T. 2003. East Anatolian high plateau as a mantle-supported, N-S shortened domal structure. Geophysical Research Letters 30, 24, 8045. Doi: 10.1029/2003GL017858

Shahbazi Shiran, H., Shafaii Moghadam, H. 2014. Geochemistry and petrogenesis of the Sabalan Plio-Quaternary volcanic rocks: Implication for post-collisional magmatism. Iranian Journal of Crystallography and Mineralogy 22, 2, 27-68.

Shaw, D.M. 1970. Trace element fractionation during anatexis. Geochimica et Cosmochimica Acta 34, 237–243

Sigurdsson, H., Houghton, B., McNutt, S.R., Rymer, H., Stix, J. 2000. Encyclopedia of Volcanoes. San Diego Academic Press, 1000 p.

Sun, S.-S., McDonough, W.F. 1989. Chemical and isotopic systematics of oceanic basalts: implications for mantle compositions and processes. In: Saunders, A.D., Norry, M.J. (Eds.), Magmatism in the Ocean Basins: Special Publication, 42. The Geological Society of London, pp. 313–345.

Thompson, R.N. 1982. Magmatism of the British tertiary volcanic province. Scotland Geological Journal 18, 49-107.

Walter, M.J. 1998. Melting of garnet peridotite and the origin of komatiite and depleted lithosphere. Journal of Petrology 39, 29–60.

Zor, E., Sandvol, E., Gürbüz, C., Türkelli, N., Seber, D. Barazangi, M. 2003. The crustal structure of the East Anatolian plateau (Turkey) from receiver functions. Geophysical Research Letters 30, 24, 8043. Doi: 10.1029/2003GL018192.